

Cite as: R. E. Baker *et al.*, *Science* 10.1126/science.abc2535 (2020).

Susceptible supply limits the role of climate in the early SARS-CoV-2 pandemic

Rachel E. Baker^{1,2*}, Wenchang Yang³, Gabriel A. Vecchi^{1,3}, C. Jessica E. Metcalf^{2,4}, Bryan T. Grenfell^{2,4,5}

¹Princeton Environmental Institute, Princeton University, Princeton, NJ, USA. ²Department of Ecology and Evolutionary Biology, Princeton University, Princeton, NJ, USA.

³Department of Geosciences, Princeton University, Princeton, NJ, USA. ⁴Woodrow Wilson School of Public and International Affairs, Princeton University, Princeton, NJ, USA. ⁵Division of International Epidemiology and Population Studies, Fogarty International Center, National Institutes of Health, Bethesda, MD, USA.

*Corresponding author. Email: racheleb@princeton.edu

Preliminary evidence suggests that climate may modulate the transmission of SARS-CoV-2. Yet it remains unclear whether seasonal and geographic variations in climate can substantially alter the pandemic trajectory, given high susceptibility is a core driver. Here, we use a climate-dependent epidemic model to simulate the SARS-CoV-2 pandemic probing different scenarios based on known coronavirus biology. We find that while variations in weather may be important for endemic infections, during the pandemic stage of an emerging pathogen the climate drives only modest changes to pandemic size. A preliminary analysis of non-pharmaceutical control measures indicates that they may moderate the pandemic-climate interaction via susceptible depletion. Our findings suggest, without effective control measures, strong outbreaks are likely in more humid climates and summer weather will not substantially limit pandemic growth.

The SARS-CoV-2 pandemic represents an unprecedented public health, social and economic challenge. Sustained local transmission is present in multiple countries, in all continents, and the implications in terms of morbidity and mortality are expected to be severe (1, 2). The role of seasonal and geographic climate variations in modulating the transmission of the virus has received increasing attention. Studies using a regression framework have found a role for temperature, relative and specific humidity in the transmission of SARS-CoV-2 (3–7), suggesting that cold, dry conditions increase the transmission of the virus. However, with limited data on the current epidemic, these early-stage results are inevitably inconclusive. Furthermore, the relative importance of climate drivers when compared to high population susceptibility during the pandemic stage of an emerging infection such as SARS-CoV-2, has not been fully characterized.

Climate affects the transmission of several directly-transmitted pathogens (8). Specific humidity (the mass of water vapor in a unit mass of moist air) has been shown to be important for influenza transmission in both laboratory settings (9–11), and in population-level studies (12). Respiratory syncytial virus (RSV), a childhood pathogen, has also been found to be dependent on specific humidity (13) and exhibits latitudinal correlations with climate (14). For both influenza and RSV, low specific humidity increases transmission and epidemics tend to peak in the wintertime in northern latitudes. However, other directly-transmitted infections exhibit different patterns (15), with enteroviruses, for instance, often peaking in the summer months (16).

Prior work on climate and directly-transmitted diseases has typically considered endemic infections, such as seasonal

influenza or RSV. Emerging pathogens, in contrast, have distinct dynamics driven by high population susceptibility (17). A key question is the extent to which seasonal and geographic climate variations are relevant in the pandemic phase of an emerging infection. Here we build on known features of endemic human coronaviruses and other directly-transmitted infections to probe this question. Although we do not yet know the climate sensitivity of SARS-CoV-2 transmission directly, data exists on four other coronaviruses that currently circulate in human populations. Two of these coronaviruses, HCoV-HKU1 and HCoV-OC43, are of the same betacoronavirus genus as SARS-CoV-2 (18).

We use data on HCoV-HKU1 and HCoV-OC43 from US census regions to understand the potential climate dependence of betacoronavirus transmission (19). We fit a Susceptible-Infected-Recovered-Susceptible (SIRS) model to case data of HCoV-HKU1 and HCoV-OC43 where the fitted parameters include the climate dependence of transmission and the length of immunity following infection. All other parameters are fixed, based on values from Kissler *et al.* 2020 (18). Motivated by the climate-dependence of influenza and RSV, we posit that transmission depends on specific humidity: we use population-weighted average climatology of specific humidity over 2014–2020 taken from the ERA5 reanalysis dataset (20), with population data from (21). We note that specific humidity is dependent on temperature via the Clausius-Clapeyron relation and results using both variables have been found to be equivalent for other diseases (13). After fitting the model parameters, we run simulations of the SARS-CoV-2 pandemic under three scenarios. In the first scenario we assume SARS-CoV-2 has the same sensitivity to climate as

influenza, based on a prior model from laboratory studies (9, 12). In the second and third scenarios, we assume SARS-CoV-2 has the same climate dependence and length of immunity as HCoV-OC43 and HCoV-HKU1 respectively. While we assume the climate dependence is the same as these three infections, our simulations use R_0 based on current estimates of SARS-CoV-2 (18, 22).

We first consider the seasonality of the endemic betacoronaviruses. Figure 1 shows the average seasonal pattern of endemic betacoronaviruses, OC43 and HKU1, for different regions in the US. Cases of both diseases increase as specific humidity declines (fig. S1). We therefore assume that to some extent transmission will decline with specific humidity, however, the extent of the decline is yet to be determined. We characterize the link between specific humidity and the transmission of SARS-CoV-2 using plausible estimates derived from the two endemic betacoronaviruses as well as influenza. Figure 1A shows different potential functional forms for the climate-transmission relationship. Changes to specific humidity modulate R_0 between a maximum wintertime value and a hypothesized lower bound, taken from prior studies (18, 22). In the extreme cases, transmission (R_0) either rapidly declines as specific humidity increases or has no relationship with specific humidity. The highlighted influenza relationship is based on laboratory studies using the guinea pig animal model (9–11), and later used to predict influenza epidemics in human populations (12). In this case R_0 values correspond to SARS-CoV-2 estimates.

The other two scenarios in Fig. 1A correspond to the relationship between climate and OC43 and HKU1 transmission. We evaluate the functional form of this relationship by fitting our climate-driven SIRS model to US case data for the two infections (Fig. 1, B and C, and figs. S2 and S3). Our results (Fig. 1, D and E) suggest a somewhat wide range of climate dependency for the two coronaviruses, with HKU1 having a much steeper response to specific humidity than OC43. Strong seasonal forcing has been linked to biennial outbreaks, as observed for HKU1 (fig. S2), in other respiratory pathogens (13) and implies endemic dynamics driven by herd immunity; however this inference may be complicated by cross-protection from other circulating strains (18). While there is some uncertainty in our estimates, simulating a pandemic outbreak using a range of climate-transmission dependencies allows us to explore a wide plausible range of potential climate effects.

We simulate a pandemic invasion for all locations (Fig. 2, A and C) and focus on the results for nine exemplar cities (Fig. 2, C to E) each with a very distinct mean and seasonal cycle of specific humidity (fig. S4). We stress that these initial simulations explore only the interaction of the epidemic (SIRS) model clockwork and seasonality in transmission; they do not address complexities of demography, control and

other environmental factors. In Fig. 2, C to E, we show the evolution of the simulated pandemic, holding population constant, for northern hemisphere, southern hemisphere and tropical locations. The model assumes the outbreak starts at the same time and no control measures are in place, revealing only the effect of climate on pandemic size and duration. For the northern hemisphere locations, we do not see any substantial difference in pandemic size across all three scenarios, despite very different climates in New York, London and Delhi. In the influenza and HKU1 scenarios, tropical locations experience a more sustained, lower intensity pandemic than the northern hemisphere. These scenarios represent a stronger dependence on climate than OC43, such that the lack of really dry conditions (low specific humidity) in tropical regions means these locations do not experience the high transmission rates of the higher latitudes. However, the outbreak in the tropical cities remains significant, and factors we do not explore here, such as population density, could further exacerbate the size of the epidemic.

We also simulate the pandemic in a range of southern hemisphere locations (Fig. 2D). We see only minor delays in the peak of southern hemisphere locations relative to the northern hemisphere (Fig. 2B), despite the six-month shift in specific humidity seasonality between the two hemispheres (fig. S4). For the OC43 scenario, pandemics are temporally aligned across all locations and of similar magnitude. A stronger climate response for influenza and HKU1 parameters leads to slight regional differences. It is worth noting that our different scenarios also reflect a range of immunity lengths. The size of the pandemic peak is not affected by changes in immunity length (fig. S11), but the timing of latter stage outbreaks is partially dictated by this parameter. The differential timing of secondary peaks in the influenza and HKU1 scenarios, which have a similar climate-dependence, is driven by this variability.

During the pandemic stage of an emerging pathogen the lack of population immunity, i.e., high susceptibility, is a crucial driver. To illustrate this in the general case, we run our simulation model for different climates (represented by the seasonal range of humidity values a location experiences) and different levels of population susceptibility, using the mean specific humidity and seasonality of New York. Figure 3, A to C, shows the results in terms of the size of the pandemic peak. While humidity range does modulate pandemic size, population susceptibility exhibits a much steeper gradient. For novel pathogens, such as SARS-CoV-2, the proportion of the population susceptible to infection may be close to 1. To illustrate the potential longer term behavior of the pandemic, we plot a typical pandemic trajectory on the SI phase plane (Fig. 3D). The initial pandemic trajectory (red) is relatively independent of seasonal forcing. This then gives way to the endemic attractor (blue) which oscillates around the equilibrium of

the unforced model (green). These longer term dynamics show a much stronger signature of seasonal forcing than the initial pandemic phase (figs. S9 and S10).

Figures 3E and 4 show a preliminary exploration of the impact of non-pharmaceutical control on the epidemic trajectory. In Fig. 3E, we show the SI phase plane where the HKU1 parameters of R_0 are artificially controlled for a six month period to $R_0 = 1.1$. In this scenario, the control measures result in a moderate reduction in peak incidence as the outbreak is shifted to the summer months, however, high susceptibility still results in a substantial numbers of cases. In Fig. 4, we explore the interaction between the climate and control measures in more detail. We consider four scenarios: climate-dependencies based on OC43 and HKU1 as well as control measures where $R_0 = 1.1$ or 1.3, representing limited transmission. For each scenario we vary the length of the control measure and the location, however for simplicity we assume all control measures start at two times, four weeks and six weeks after the disease is introduced. We note that these control measures are simplified test cases and do not represent the local heterogeneity and efficacy of current controls, which is yet to be determined. These results show change to peak incidence, changes to number infected are shown in fig. S5.

For all control scenarios we assume a degree of transmission during the control period, such that $R_0 > 1$, resulting in an increase in population immunity over time. In the scenarios where $R_0 = 1.3$, immunity builds faster and control measures work to reduce the pandemic peak after several months. In the $R_0 = 1.1$ scenario more time is required for population immunity to build such that the pandemic peak is reduced across all locations. In this scenario, as susceptibility declines, the climate plays a more substantial role in determining pandemic peak size (Fig. 4, A and B). When $R_0 = 1.1$ in both the HKU1 and OC43 scenarios, releasing control measures close to the month of maximum transmission may result in a larger pandemic peak compared to the no control scenario, particularly in the higher latitudes where transmission likely increases in the winter (fig. S6).

More broadly, our simulated control measures imply that the key determinant of reduced peak incidence is the extent to which population immunity builds over the control period, demonstrated by the higher efficacy of the $R_0 = 1.3$ control scenario in mitigating peak incidence. The climate plays a complex role in tuning the efficacy of potential control efforts, resulting in differential outcomes depending on location, however population susceptibility remains a fundamental driver. Further exploration of these complexities may be necessary when evaluating location-specific controls. The timing of introduction and the efficacy of local control measures as well as factors such as population density and contact patterns could also shape future outcomes.

Serological surveys, at the local level, will be important for tracking the build up of immunity over time. Moreover, implementing control measures buys crucial time while vaccine and other treatments are developed.

There are several caveats to interpreting these results. Primarily, these simulations do not address location specific factors such as spatial and social mixing patterns, contact networks, population density and the specifics of control timing and efficacy. In particular, our results apply most closely to relatively well-mixed epidemics in large cities. Rural areas (with potentially lower R_0 ; see figs. S7 and S8), may have a more delayed initial epidemic with complex consequences for ensuing interactions with climate drivers. Our model also does not account for potential cross-protection from other coronavirus infections (18). Cross-immunity may contribute to the seasonality of endemic coronaviruses, meaning estimated climate drivers could be even weaker than we suggest and our main findings, conservative (16, 23). Finally, results from influenza and RSV suggest that high precipitation may play a role in driving transmission (13, 24), particularly in tropical locations. Due to limited data on betacoronaviruses from tropical locations, we have not been able to confirm whether a rainfall signal exists. Precipitation effects and other drivers such as schooling may also impact the epidemic trajectory, particularly post-pandemic. We further test for the sensitivity of our results to changes in core parameter values (materials and methods and figs. S7 to S11). These analyses suggest our results are qualitatively robust to variations in climate dependency and weather fluctuations.

Our results suggest that while climate may play a role in modulating detailed aspects of the size and timescales of a pandemic outbreak within a particular location, population immunity is a much more fundamental driver of pandemic invasion dynamics. Although our HKU1 scenarios presents a modest role for climate in terms of shifting the timing and intensity of the pandemic, a scenario with OC43 parameters is equally likely. In terms of the SARS-CoV-2 pandemic, our results imply that both tropical and temperate locations should prepare for severe outbreaks of the disease and that summertime temperatures will not effectively limit the spread the infection. However, this does not mean the climate is not important in the longer term. Endemic cycles of the disease will likely be tied to climate factors and seasonal peaks may vary with latitude (figs. S3, S9, and S10). A more detailed understanding of climate drivers as well as immunity length will be crucial for understanding the implications of control measures. Furthermore, weather and near-term climate forecasts could be helpful for predicting secondary outbreaks after the initial pandemic phase has passed.

REFERENCES AND NOTES

1. R. Verity, L. C. Okell, I. Dorigatti, P. Winskill, C. Whittaker, N. Imai, G. Cuomo-Dannenburg, H. Thompson, P. Walker, H. Fu, A. Dighe, J. Griffin, A. Cori, M.

- Baguelin, S. Bhatia, A. Boonyasiri, Z. M. Cucunuba, R. Fitzjohn, K. A. M. Gaythorpe, W. Green, A. Hamlet, W. Hinsley, D. Laydon, G. Nedjati-Gilani, S. Riley, S. van-Elsand, E. Volz, H. Wang, Y. Wang, X. Xi, C. Donnelly, A. Ghani, N. Ferguson, Estimates of the severity of COVID-19 disease. medRxiv 2020.03.09.20033357 [Preprint]. 13 March 2020; <https://doi.org/10.1101/2020.03.09.20033357>.
2. R. Li, C. Rivers, Q. Tan, M. B. Murray, E. Toner, M. Lipsitch, The demand for inpatient and ICU beds for COVID-19 in the US: lessons from Chinese cities. medRxiv 2020.03.09.20033241 [Preprint]. 16 March 2020; <https://doi.org/10.1101/2020.03.09.20033241>.
3. Q. Bukhari, Y. Jameel, Will coronavirus pandemic diminish by summer? SSRN 3556998 [Preprint]. 17 March 2020; <https://dx.doi.org/10.2139/ssrn.3556998>.
4. J. Wang, K. Tang, K. Feng, W. Lv, High temperature and high humidity reduce the transmission of COVID-19. SSRN 3551767 [Preprint]. 9 March 2020; <https://dx.doi.org/10.2139/ssrn.3551767>.
5. M. M. Sajadi, P. Habibzadeh, A. Vintzileos, S. Shokouhi, F. Miralles-Wilhelm, A. Amoroso, Temperature, humidity and latitude analysis to predict potential spread and seasonality for COVID-19. SSRN 3550308 [Preprint]. 5 March 2020; <https://dx.doi.org/10.2139/ssrn.3550308>.
6. W. Luo, M. S. Majumder, D. Liu, C. Poirier, K. D. Mandl, M. Lipsitch, M. Santillana, The role of absolute humidity on transmission rates of the COVID-19 outbreak. medRxiv 2020.02.12.20022467 [Preprint]. 17 February 2020; <https://doi.org/10.1101/2020.02.12.20022467>.
7. Y. Ma, Y. Zhao, J. Liu, X. He, B. Wang, S. Fu, J. Yan, J. Niu, B. Luo, Effects of temperature variation and humidity on the mortality of COVID-19 in Wuhan. medRxiv 2020.03.15.20036426 [Preprint]. 18 March 2020; <https://doi.org/10.1101/2020.03.15.20036426>.
8. R. E. Baker, A. S. Mahmud, C. J. E. Metcalf, Dynamic response of airborne infections to climate change: Predictions for varicella. *Clim. Change* **148**, 547–560 (2018). doi:[10.1007/s10584-018-2204-4](https://doi.org/10.1007/s10584-018-2204-4)
9. J. Shaman, M. Kohn, Absolute humidity modulates influenza survival, transmission, and seasonality. *Proc. Natl. Acad. Sci. U.S.A.* **106**, 3243–3248 (2009). doi:[10.1073/pnas.0806852106](https://doi.org/10.1073/pnas.0806852106) Medline
10. A. C. Lowen, J. Steel, Roles of humidity and temperature in shaping influenza seasonality. *J. Virol.* **88**, 7692–7695 (2014). doi:[10.1128/JVI.03544-13](https://doi.org/10.1128/JVI.03544-13) Medline
11. A. C. Lowen, S. Mubareka, J. Steel, P. Palese, Influenza virus transmission is dependent on relative humidity and temperature. *PLOS Pathog.* **3**, 1470–1476 (2007). doi:[10.1371/journal.ppat.0030151](https://doi.org/10.1371/journal.ppat.0030151) Medline
12. J. Shaman, V. E. Pitzer, C. Viboud, B. T. Grenfell, M. Lipsitch, Absolute humidity and the seasonal onset of influenza in the continental United States. *PLOS Biol.* **8**, e1000316 (2010). doi:[10.1371/journal.pbio.1000316](https://doi.org/10.1371/journal.pbio.1000316) Medline
13. R. E. Baker, A. S. Mahmud, C. E. Wagner, W. Yang, V. E. Pitzer, C. Viboud, G. A. Vecchi, C. J. E. Metcalf, B. T. Grenfell, Epidemic dynamics of respiratory syncytial virus in current and future climates. *Nat. Commun.* **10**, 5512 (2019). doi:[10.1038/s41467-019-13562-y](https://doi.org/10.1038/s41467-019-13562-y) Medline
14. V. E. Pitzer, C. Viboud, W. J. Alonso, T. Wilcox, C. J. Metcalf, C. A. Steiner, A. K. Haynes, B. T. Grenfell, Environmental drivers of the spatiotemporal dynamics of respiratory syncytial virus in the United States. *PLOS Pathog.* **11**, e1004591 (2015). doi:[10.1371/journal.ppat.1004591](https://doi.org/10.1371/journal.ppat.1004591) Medline
15. M. E. Martinez, The calendar of epidemics: Seasonal cycles of infectious diseases. *PLOS Pathog.* **14**, e1007327 (2018). doi:[10.1371/journal.ppat.1007327](https://doi.org/10.1371/journal.ppat.1007327) Medline
16. S. Takahashi, Q. Liao, T. P. Van Boeckel, W. Xing, J. Sun, V. Y. Hsiao, C. J. E. Metcalf, Z. Chang, F. Liu, J. Zhang, J. T. Wu, B. J. Cowling, G. M. Leung, J. J. Farrar, H. R. van Doorn, B. T. Grenfell, H. Yu, Hand, foot, and mouth disease in China: Modeling epidemic dynamics of enterovirus serotypes and implications for vaccination. *PLOS Med.* **13**, e1001958 (2016). doi:[10.1371/journal.pmed.1001958](https://doi.org/10.1371/journal.pmed.1001958) Medline
17. J. R. Gog, S. Ballesteros, C. Viboud, L. Simonsen, O. N. Bjornstad, J. Shaman, D. L. Chao, F. Khan, B. T. Grenfell, Spatial transmission of 2009 pandemic influenza in the US. *PLOS Comput. Biol.* **10**, e1003635 (2014). doi:[10.1371/journal.pcbi.1003635](https://doi.org/10.1371/journal.pcbi.1003635) Medline
18. S. M. Kissler, C. Tedijanto, E. Goldstein, Y. H. Grad, M. Lipsitch, Projecting the transmission dynamics of SARS-CoV-2 through the postpandemic period. *Science* eabb5793 (2020). doi:[10.1126/science.abb5793](https://doi.org/10.1126/science.abb5793) Medline
19. Centers for Disease Control and Prevention, Surveillance for common human coronaviruses (2020); www.cdc.gov/surveillance/nrevss/coronavirus/index.html.
20. L. Hoffmann, G. Günther, D. Li, O. Stein, X. Wu, S. Griessbach, Y. Heng, P. Konopka, R. Müller, B. Vogel, J. S. Wright, From ERA-Interim to ERA5: The considerable impact of ECMWF's next-generation reanalysis on Lagrangian transport simulations. *Atmos. Chem. Phys.* **19**, 3097–3124 (2019). doi:[10.5194/acp-19-3097-2019](https://doi.org/10.5194/acp-19-3097-2019)
21. NASA Socioeconomic Data and Applications Center (SEDAC), Gridded Population of the World, Version 4 (GPWv4): Population Density, Revision 11. Palisades, NY; <https://sedac.ciesin.columbia.edu/data/set/gpw-v4-population-density-rev11> [accessed March 2020].
22. S. W. Park, B. M. Bolker, D. Champredon, D. J. D. Earn, M. Li, J. S. Weitz, B. T. Grenfell, J. Dushoff, Reconciling early-outbreak estimates of the basic reproductive number and its uncertainty: framework and applications to the novel coronavirus (SARS-CoV-2) outbreak. medRxiv 2020.01.30.20019877 [Preprint]. 28 February 2020; <https://doi.org/10.1101/2020.01.30.20019877>.
23. M. Kamo, A. Sasaki, The effect of cross-immunity and seasonal forcing in a multi-strain epidemic model. *Physica D* **165**, 228–241 (2002). doi:[10.1016/S0167-2789\(02\)00389-5](https://doi.org/10.1016/S0167-2789(02)00389-5)
24. J. D. Tamerius, J. Shaman, W. J. Alonso, K. Bloom-Feshbach, C. K. Uejio, A. Comrie, C. Viboud, Environmental predictors of seasonal influenza epidemics across temperate and tropical climates. *PLOS Pathog.* **9**, e1003194 (2013). doi:[10.1371/journal.ppat.1003194](https://doi.org/10.1371/journal.ppat.1003194) Medline
25. R. E. Baker, rebaker64/climate-cov: R1. Zenodo (2020); doi:[10.5281/zenodo.3787766](https://doi.org/10.5281/zenodo.3787766).
26. M. E. Killerby, H. M. Biggs, A. Haynes, R. M. Dahl, D. Mustaquin, S. I. Gerber, J. T. Watson, Human coronavirus circulation in the United States 2014–2017. *J. Clin. Virol.* **101**, 52–56 (2018). doi:[10.1016/j.jcv.2018.01.019](https://doi.org/10.1016/j.jcv.2018.01.019) Medline
27. R. Gelaro, W. McCarty, M. J. Suárez, R. Todling, A. Molod, L. Takacs, C. Randles, A. Darmenov, M. G. Bosilovich, R. Reichle, K. Wargan, L. Coy, R. Cullather, C. Draper, S. Akella, V. Buchard, A. Conaty, A. da Silva, W. Gu, G.-K. Kim, R. Koster, R. Lucchesi, D. Merkova, J. E. Nielsen, G. Partyka, S. Pawson, W. Putman, M. Rienecker, S. D. Schubert, M. Sienkiewicz, B. Zhao, The Modern-Era Retrospective Analysis for Research and Applications, Version 2 (MERRA-2). *J. Clim.* **30**, 5419–5454 (2017). doi:[10.1175/JCLI-D-16-0758.1](https://doi.org/10.1175/JCLI-D-16-0758.1) Medline
28. L. Bao, W. Deng, H. Gao, C. Xiao, J. Liu, J. Xue, Lv. Qi, J. Liu, P. Yu, Y. Xu, F. Qi, Y. Qu, F. Li, Z. Xiang, H. Yu, S. Gong, M. Liu, G. Wang, S. Wang, Z. Song, Y. Liu, W. Zhao, Y. Han, L. Zhao, X. Liu, Q. Wei, C. Qin, Lack of reinfection in rhesus macaques infected with SARS-CoV-2. bioRxiv 2020.03.13.3990226 [Preprint]. 1 May 2020; <https://doi.org/10.1101/2020.03.13.3990226>.
29. K. A. Callow, H. F. Parry, M. Sergeant, D. A. Tyrrell, The time course of the immune response to experimental coronavirus infection of man. *Epidemiol. Infect.* **105**, 435–446 (1990). doi:[10.1017/S0950268800048019](https://doi.org/10.1017/S0950268800048019) Medline

ACKNOWLEDGMENTS

Funding: REB is supported by the Cooperative Institute for Modelling the Earth System (CIMES). WY is supported by Princeton Environmental Institute/Princeton Institute for International and Regional Studies. **Author contributions:** Conceptualization: REB, WY, GAV, CJEM, BTG; Data curation: REB, WY; Formal analysis: REB; Methodology: REB, WY, GAV, CJEM, BTG; Software: REB, WY, GV; Visualization: REB, GV; Writing, original draft: REB; Writing, reviewing and editing: REB, WY, GAV, CJEM, BTG. **Competing interests:** The authors declare no competing interests. **Data and materials availability:** US coronavirus data are available from the The National Respiratory and Enteric Virus Surveillance System (NREVSS) on request: <https://www.cdc.gov/surveillance/nrevss/coronavirus/index.html>. Climate data are publicly available from ERA5 and NASA; ERA5 data: <https://www.ecmwf.int/en/forecasts/datasets/reanalysis-datasets/era5> and NASA MERRA data: <https://gmao.gsfc.nasa.gov/reanalysis/MERRA/>. Code for running the model is available via [github/rebaker64/climate-cov](https://github.com/rebaker64/climate-cov) (25). This work is licensed under a Creative Commons Attribution 4.0 International (CC BY 4.0) license, which permits unrestricted use, distribution, and reproduction in any medium, provided the original work is properly cited. To view a copy of this license, visit <https://creativecommons.org/licenses/by/4.0/>. This license does not apply to figures/photos/artwork or other content included in the article that is credited to a third party; obtain authorization from the rights holder before using such material.

SUPPLEMENTARY MATERIALS

science.scienmag.org/cgi/content/full/science.abc2535/DC1

Materials and Methods

Figs. S1 to S11

References (26–29)

MDAR Reproducibility Checklist

15 April 2020; accepted 14 May 2020

Published online 18 May 2020

10.1126/science.abc2535

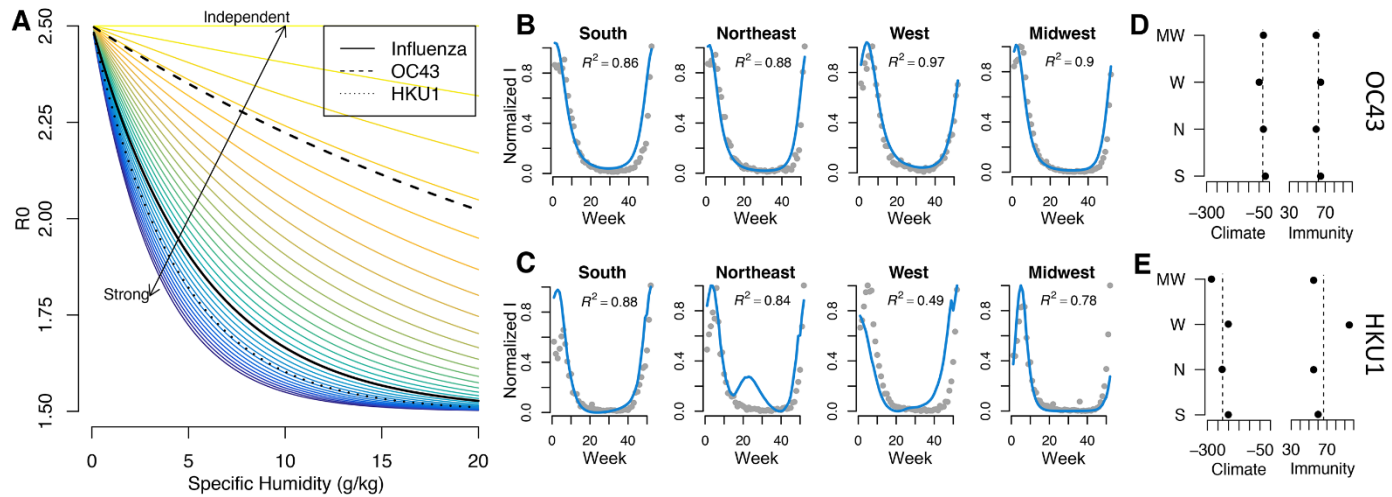


Fig. 1. Specific humidity and transmission. (A) Colored lines represent different hypotheses for the relationship between climate and transmission for SARS-CoV-2. Values of R_0 reflect SARS-CoV-2 estimates and the functional climate-dependence of influenza transmission, OC43 transmission and HKU1 transmission is shown with black lines. (B and C) A summary of seasonal model fits (blue line) for scaled average weekly cases (grey) of OC43 (B) and HKU1 (C) (our model captures the biennial cycles of HKU1, shown in fig. S3 and detailed model fits for OC43 shown in fig. S2). R^2 values are shown inset. (D and E) Fit results in terms of climate-dependence and immunity length (weeks) for OC43 (D) and HKU1 (E), where mean fits are shown with dashed lines.

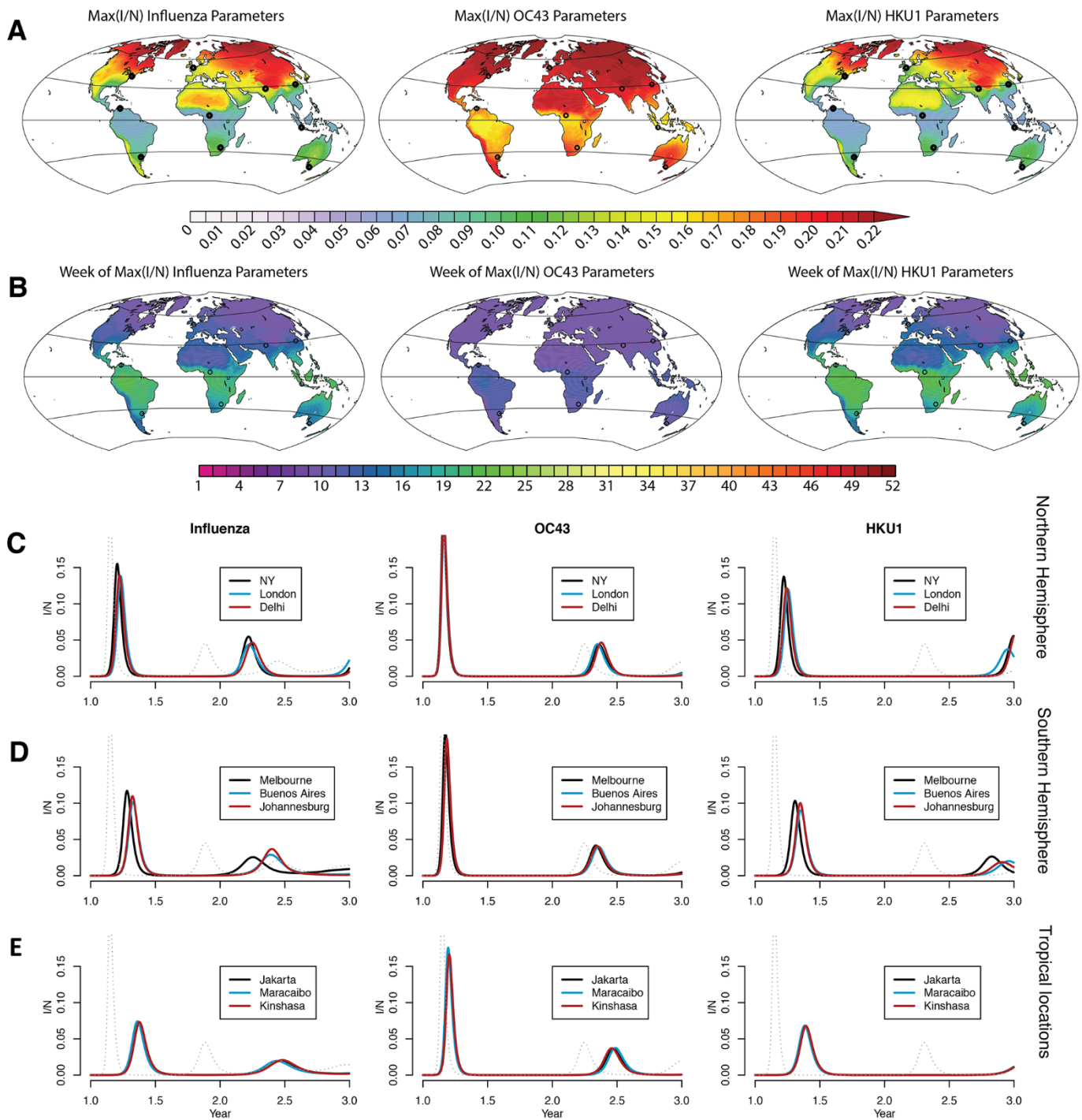


Fig. 2. Global model results and nine example trajectories. (A and B) Maximum I/N (A) and the timing of peak incidence (B) for global locations. Black circles show locations where trajectories are explicitly shown. (C to E) Simulated pandemics are shown for cities in the northern hemisphere (C), the southern hemisphere (D), and tropical locations (E). The dotted line represents a pandemic with no climate dependence.

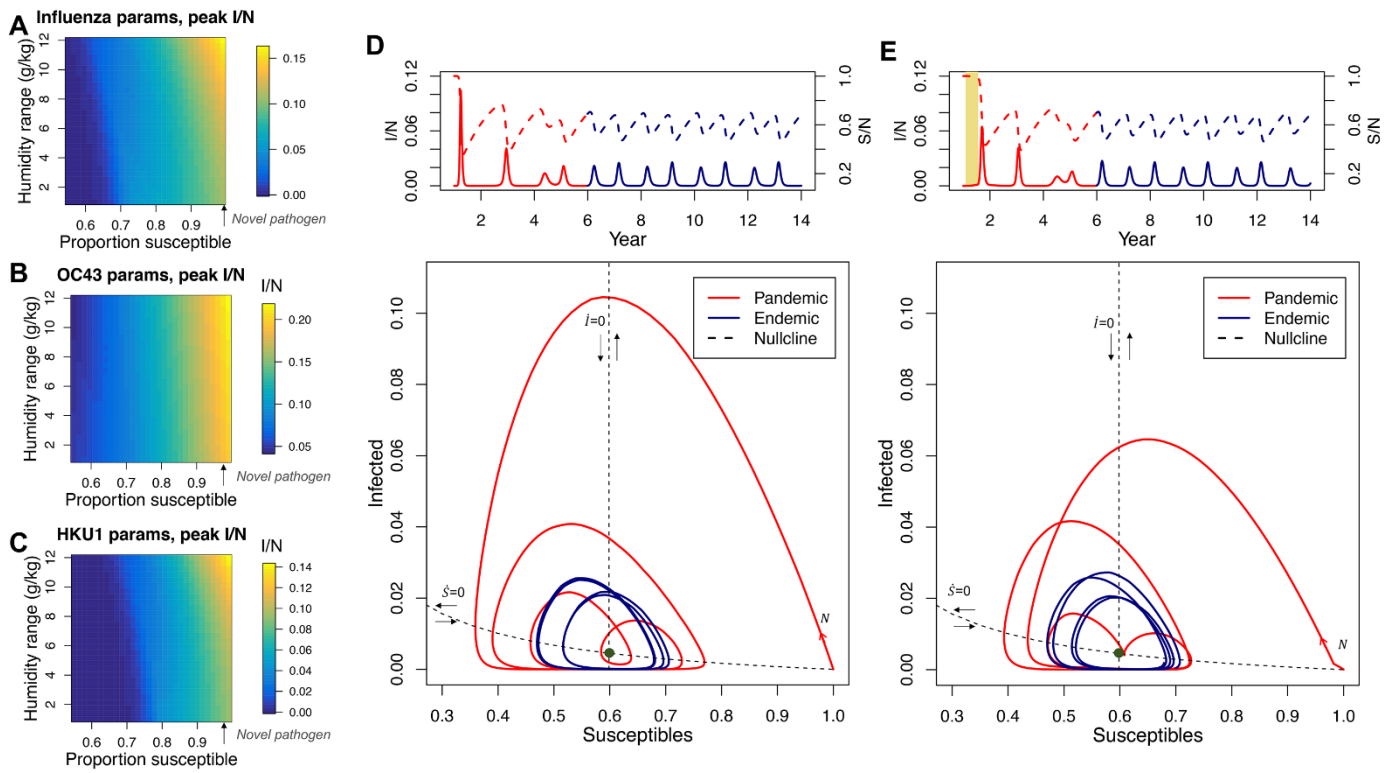


Fig. 3. Pandemic peak size depends on proportion susceptible. (A to C) For the three scenarios, influenza (A), OC43 (B), and HKU1 (C), the surface plot shows the dependence of maximum pandemic incidence/capita on seasonal range of humidity and proportion of population susceptible, assuming mean humidity of New York. (D) The time series from pandemic to endemic outbreaks for an example location (Wuhan with HKU1 params) (top) and the equivalent SI phase plane of pandemic and epidemic trajectories (bottom). The two nullclines are from the unforced SIRS using mean R_0 . The green circle represents the equilibrium of the unforced model. (E) The same trajectory but with a six month control period (reducing R_0 to 1.1).

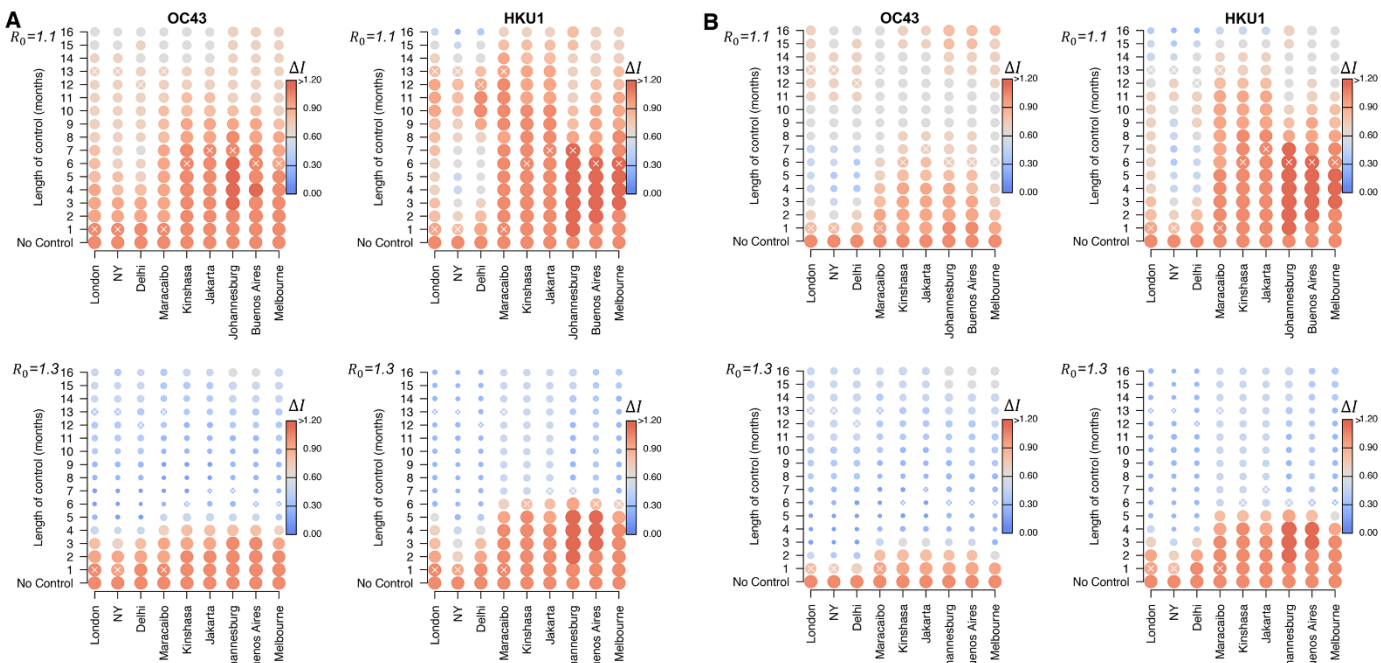


Fig. 4. Interaction between control measures and the climate. (A and B) Four scenarios representing the interaction of different climate-dependencies (OC43 and HKU1 params) with two potential control measures [$R_0 = 1.1$ and 1.3 in the control period, occurring one month (A) and six weeks (B) after pandemic start]. Size and color of the circle represents the size of peak incidence (within two years of pandemic start) relative to the no-control scenario. White crosses show month of maximum climate-driven transmission i.e., lowest specific humidity.

Susceptible supply limits the role of climate in the early SARS-CoV-2 pandemic

Rachel E. Baker, Wenchang Yang, Gabriel A. Vecchi, C. Jessica E. Metcalf and Bryan T. Grenfell

published online May 18, 2020

ARTICLE TOOLS

<http://science.science.org/content/early/2020/05/15/science.abc2535>

SUPPLEMENTARY MATERIALS

<http://science.science.org/content/suppl/2020/05/15/science.abc2535.DC1>

RELATED CONTENT

<http://stm.science.org/content/scitransmed/12/541/eabb5883.full>
<http://stm.science.org/content/scitransmed/12/534/eabb1469.full>
<http://stm.science.org/content/scitransmed/11/499/eaat0360.full>
<http://stm.science.org/content/scitransmed/9/396/eaal3653.full>

REFERENCES

This article cites 23 articles, 9 of which you can access for free
<http://science.science.org/content/early/2020/05/15/science.abc2535#BIBL>

PERMISSIONS

<http://www.science.org/help/reprints-and-permissions>

Use of this article is subject to the [Terms of Service](#)

Science (print ISSN 0036-8075; online ISSN 1095-9203) is published by the American Association for the Advancement of Science, 1200 New York Avenue NW, Washington, DC 20005. The title *Science* is a registered trademark of AAAS.

Copyright © 2020 The Authors, some rights reserved; exclusive licensee American Association for the Advancement of Science. No claim to original U.S. Government Works

Supplementary Materials for
**Susceptible supply limits the role of climate in the
early SARS-CoV-2 pandemic**

Rachel E. Baker*, Wenchang Yang, Gabriel A. Vecchi, C. Jessica E. Metcalf, Bryan T. Grenfell

*Corresponding author. Email: racheleb@princeton.edu

Published 18 May 2020 on *Science* First Release
DOI: 10.1126/science.abc2535

This PDF file includes:

Materials and Methods
Figs. S1 to S11
References

Other Supporting Online Material for this manuscript includes the following:
(available at science.sciencemag.org/cgi/content/full/science.abc2535/DC1)

MDAR Reproducibility Checklist (.pdf)

Materials and Methods

Data

Data on endemic coronaviruses come from The National Respiratory and Enteric Virus Surveillance System (NREVSS) (19) and are available on application after signing a data-use agreement with the Center for Disease Control. NREVSS is a passive surveillance network, established by the CDC that collects data from multiple laboratories across the US (25). The dataset contains the number of total weekly tests and the number of positive tests for each of the four coronavirus strains: HKU1, OC43, NL63, 229E. However, no details are provided on the number or location of reporting laboratories each week and year-to-year changes in reporting are possible. To partially correct for this, we calculate percentage positive cases for HKU1 and OC43 and following (18), we multiply this number by the proportion of weekly ILI visits obtained from the US Outpatient Influenza-like Illness Surveillance Network (ILINet). Given year-to-year variability may still not be reflective of true variability in coronavirus cases, we fit our model using only mean climatology to capture broad patterns of seasonal dynamics and timing.

Climate data for the US regions come from ERA5 (20) and population-weighted averages of specific humidity over the census region area are constructed using 2015 population data from CIESIN (21). We calculate the average climatology for 2014-2020 to run the model and do not consider year-to-year climate variations. For simulating global pandemics, we calculate a 30 year climatology using specific humidity from NASA's Modern-Era Retrospective analysis for Research and Applications (MERRA) dataset (27).

Model

The climate-driven SIRS model is based on (12):

$$\frac{dS}{dT} = \frac{N - S - I}{L} - \frac{\beta(t)IS}{N} \quad (1)$$

$$\frac{dI}{dT} = \frac{\beta(t)IS}{N} - \frac{I}{D} \quad (2)$$

where S is the susceptible population, I is the number of infectious individuals and N is the population. L represents the duration of immunity and D is the mean infectious period (fixed at 5 days). $\beta(t)$ is the contact rate at time t and is related to the basic reproductive number by $R_0(t) = \beta(t)D$. R_0 is related to specific humidity $q(t)$ using the equation:

$$R_0(t) = \exp(a * q(t) + \log(R_{0max} - R_{0min})) + R_{0min} \quad (3)$$

where a is the climate dependence parameter and R_{0max} , R_{0min} are the maximum and minimum reproductive numbers respectively.

Fitting the model

For OC43 and HKU1 we find a and L by fitting the model to data from census regions in the US. We take the average fit across census regions to represent the OC43 and HKU1 values of a and L . In general, parameter values for each disease show agreement across census regions. The western region is a slight outlier for both diseases. As this region pools data from both Alaska and Hawaii (as well as western US states) it represents a large range of climatologies and this likely makes the true climate effect harder to disentangle.

We fit over a range of climate dependencies reflecting no climate dependence to approximately double the known climate dependence on influenza [0,300]. The immunity length of SARS-CoV-2 is yet to be determined, however, some early stage research found that rhesus macaques could not be reinfected 30 days post-infection (28). Studies using another endemic

coronavirus, NL63, found that neutralizing antibody titers declined to zero 52 weeks after first infection (29). Using the US betacoronavirus data, another modelling effort found an immunity length of 40 weeks (18). Here, we assume 20 weeks in the lower bound on immunity length, and allow the model to fit a maximum immunity length of two years. Our fitted immunity lengths, L , are 62.5 and 66.25 weeks for OC43 and HKU1 respectively. Our fitted values for a are -32.5 and -227.5 for OC43 and HKU1 respectively. Visualization of the fitting process is shown in Fig. S2 and S3. For influenza, we use climate dependencies from earlier work (12), where a is -180 and L we fix at 40 weeks. Immunity for influenza is complicated by the evolution of the virus, however, 40 weeks leads to annual outbreaks without biennial dynamics and therefore provides a representation of influenza type-dynamics.

When fitting the model we use $R_{0min} = 1.2$, $R_{0max} = 2$, where R_{0min} represents a 40% reduction for R_{0max} , which is consistent with a potential maximum climate effect in other studies (18,20). We find these values of R_{0min} and R_{0max} are able to capture both the annual and biennial dynamics of OC43 and HKU1 respectively. When simulating a SARS-CoV-2 outbreak, we assume a slightly larger R_0 , corresponding to preliminary studies of the outbreak.

We run the model for fifty years to remove initial transient dynamics before fitting to case data. For the endemic model, to more accurately capture longer term susceptible dynamics, we assume a birth rate equal to the average weekly birth rate in the US between 2013 and 2020 taken from World Bank data. We set the birth rate equal to the mortality rate. We scale the model output to the census region data by first dividing both time series by the range of weekly cases and then set the model mean cases equal to the region data. This assumes a constant reporting rate for each region. Scaled data is shown in Figure S2 and Figure S3. Our fit statistic is the sum of the absolute errors. To avoid overfitting to zero cases and low level stochastic observations, for instance at the start of the time series, we only measure errors when scaled cases exceed 5%. This ensures our models captures broadly peak timing and dynamics.

Model simulations

For simulations of SARS-CoV-2, we assume the climate modulates R_0 between a maximum of 2.5 and a minimum of 1.5, representing a 40% reduction in transmission at maximum (18,20). Prior work for the endemic coronaviruses suggests a lower R_{0max} of 2.2 (18), however, early reports for SARS-CoV-2 suggest higher values, closer to 2.9 (22). Here we choose a $R_{0max} = 2.5$ as a conservative upper bound. Only locations with very dry conditions (low specific humidity) will experience R_{0max} close to this limit. Model results using other R_0 values are shown in the sensitivity analysis. We do not consider birth rates when simulating the pandemic outbreak. Birth rates do not likely contribute to susceptible dynamics over the short-run and may complicate the interpretation of regional climate differences. In all simulations unless otherwise stated the model simulation starts on day 1 of the year, assuming 1/8e06 infected, no recovered and N-I susceptible.

In some analyses, we simulate the model in the general case using a sinusoidal function to capture seasonality in specific humidity. The sine function has the mean and temporal pattern of New York specific humidity, but the range of humidity values is allowed to vary.

Sensitivity analysis

The dependence of SARS-CoV-2 transmission on the climate is fundamentally unknown. Our three scenarios (influenza, OC43 and HKU1) represent a wide range of potential climate dependencies, with HKU1 showing more substantial variations in peak incidence across regions, and OC43 showing very little. Using these parameters, our simulations predict significant outbreaks across all locations. We further test the sensitivity of our results to potential changes in climate dependence, immunity length, R_0 and weather variability.

In Fig. S7, we run simulations varying the strength of climate dependence (from double our maximum estimated value to 0) and the humidity range (assuming mean humidity and seasonal

timing of New York). Across columns we vary the starting fraction of susceptibles from 1 to 0.7. Across rows we consider different values for minimum and maximum R_0 with scenarios representing our current values for SARS-CoV-2, values from (18), our endemic coronavirus values, and a more extreme scenario where $R_{0min} = 1$. The time series show a five year simulation for New York and Jakarta with the HKU1 (strong) climate dependence and starting susceptibility at 0.7 or 1.

In all cases, comparing across columns, reducing susceptibility to 0.7 substantially reduced pandemic peak size in the first year. Scenario b), where $R_{0max} = 2, R_{0min} = 1.2$ results in smaller outbreaks in both New York and Jakarta, though the size of the outbreaks relative to each other are similar to our baseline scenario, suggesting that even with these lower R_0 values, if a large outbreak occurs in New York, a similar sized outbreak may occur in this more tropical city. The only case where outbreaks do not occur in tropical regions is scenario d), when high specific humidity lowers R_0 to 1. In Fig. S8, we further test these implications of R_{0min} . In this analysis we fix $R_{0max} = 2.5$ and vary R_{0min} as a percentage reduction in R_{0max} . For the weak climate dependence scenario, OC43, changes to R_{0min} have minimal affect on peak size. For HKU1, when $R_{0min} \leq 1$, outbreaks do not occur in tropical locations.

We also consider the effect of different weather variability on pandemic peak size. Our main model uses mean specific humidity over a 30 year period, however this long-run mean smooths over the potential impact of year-to-year weather variability. We run our model using each individual year from the MERRA dataset, repeating the weather from that year for a 10 year period. Fig S9 and S10 show the results for HKU1 and OC43 parameters respectively. We find that across a range of locations, changes to weather variability do not alter the timing or intensity of the pandemic peak. However, endemic cycles exhibit much higher sensitivity to weather variation.

Finally, we also consider the potential effect of immunity length on pandemic peak size (Fig

S11). Immunity length does not influence the size of the pandemic peak, though will impact the timing of latter stage outbreaks.

Supplemental Figures

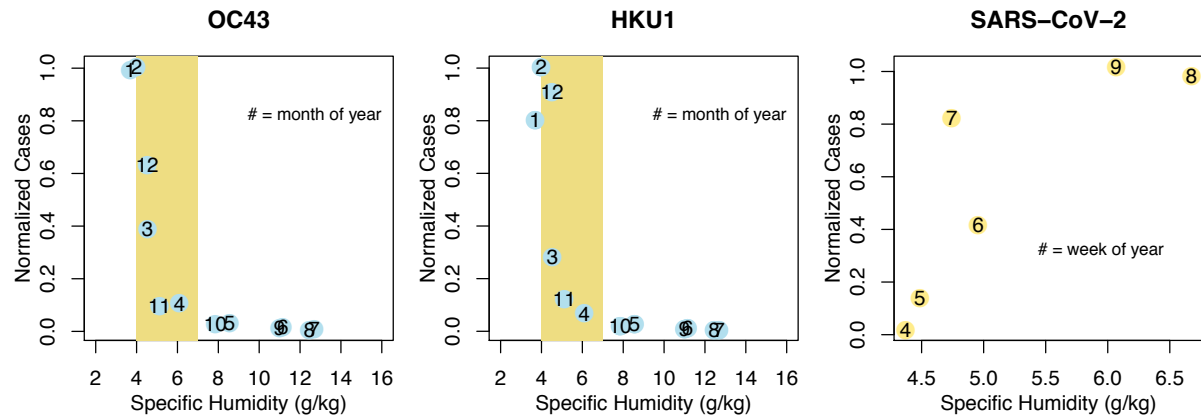


Figure S1: Seasonality of coronaviruses. Average monthly specific humidity plotted against normalized (between 0 and 1) cases of OC43 and HKU1 averaged across the US from 2014-2020, as well as normalized cases of SARS-CoV-2 in Wuhan from weeks 4-9 of 2020 (based on the time series available from the John Hopkins Coronavirus resource center at the time of access). The yellow shaded area in the first two plots corresponds to the width of the x-axis in the final plot, for comparison.

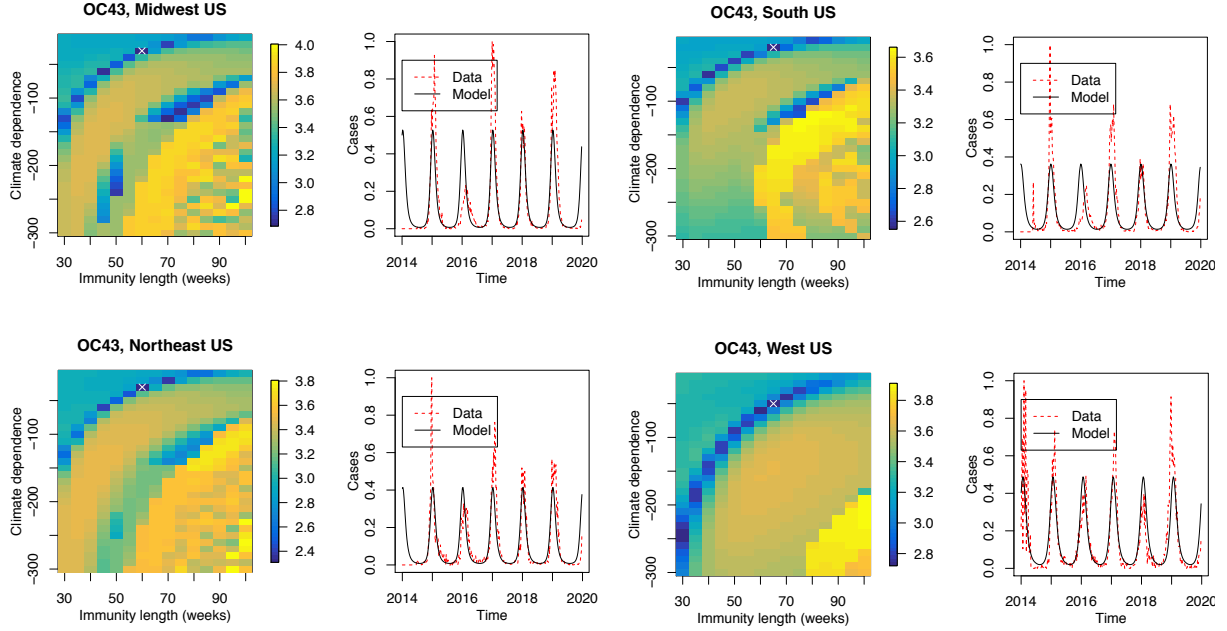


Figure S2: Model fit for OC43. Two parameters are fitted (climate dependence and immunity length) using case data for OC43 in four US census regions. Our model fits only the average seasonality of OC43 cases and does not take into account year-to-year variation. The surface plot shows the (logged) sum of absolute error. Darker regions represent a better fit of our model and the best fit parameters are shown with a white cross.

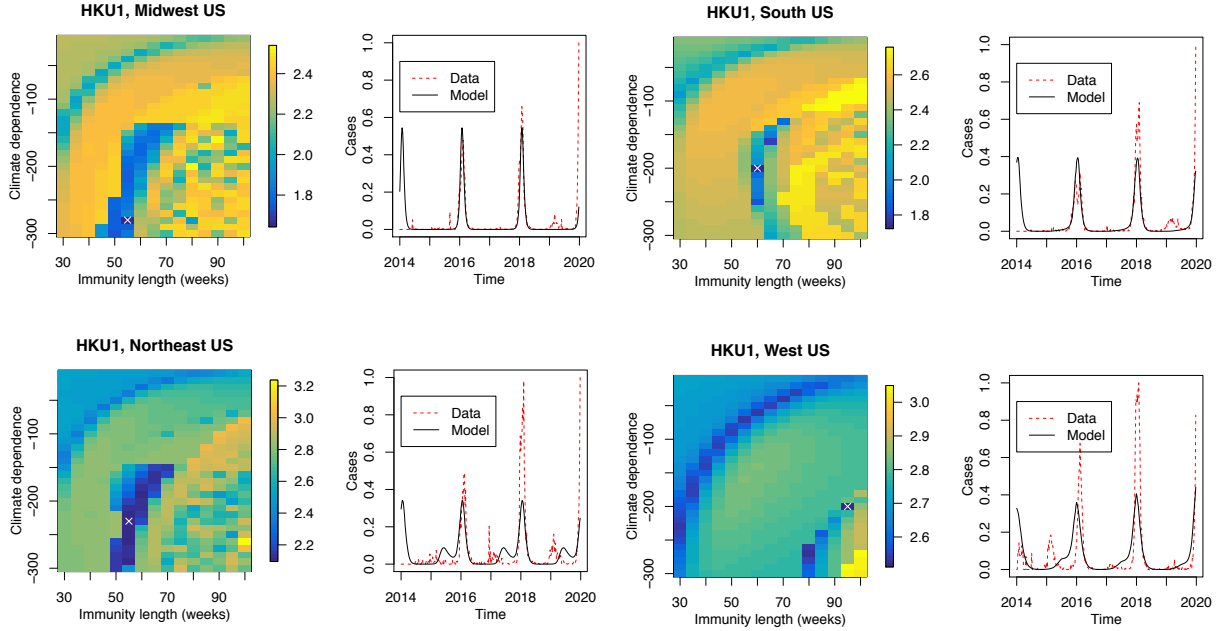


Figure S3: Model fit for HKU1. Two parameters are fitted (climate dependence and immunity length) using case data for HKU1 in four US census regions. Our model fits only the average seasonality of HKU1 cases and does not take into account year-to-year variation. The surface plot shows the (logged) sum of absolute error. Darker regions represent a better fit of our model and the best fit parameters are shown with a white cross.

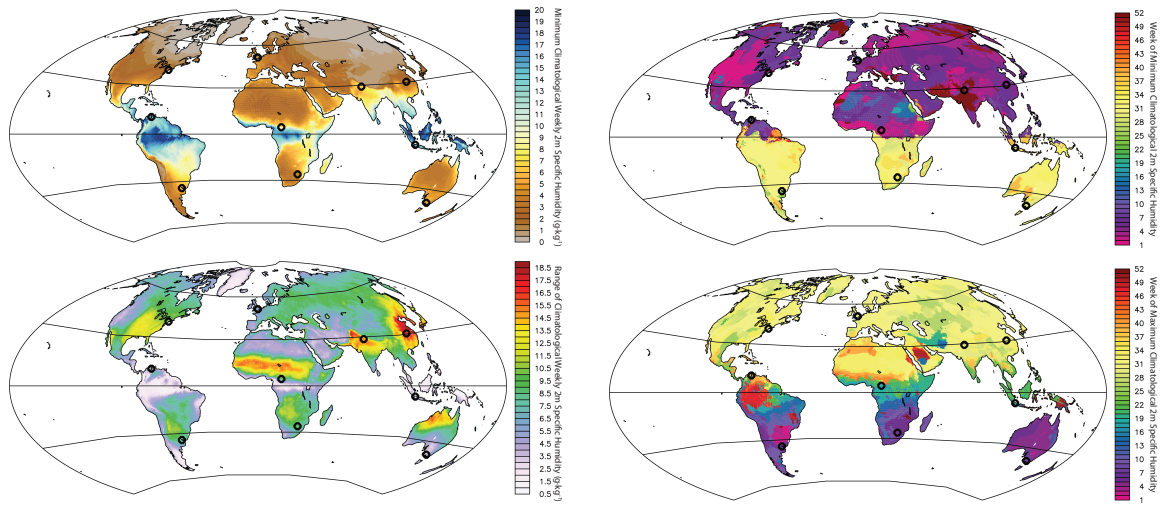


Figure S4: Specific humidity climatology. Minimum specific humidity and range of specific humidity as well as timing of minimum and maximum specific humidity is shown for the globe.

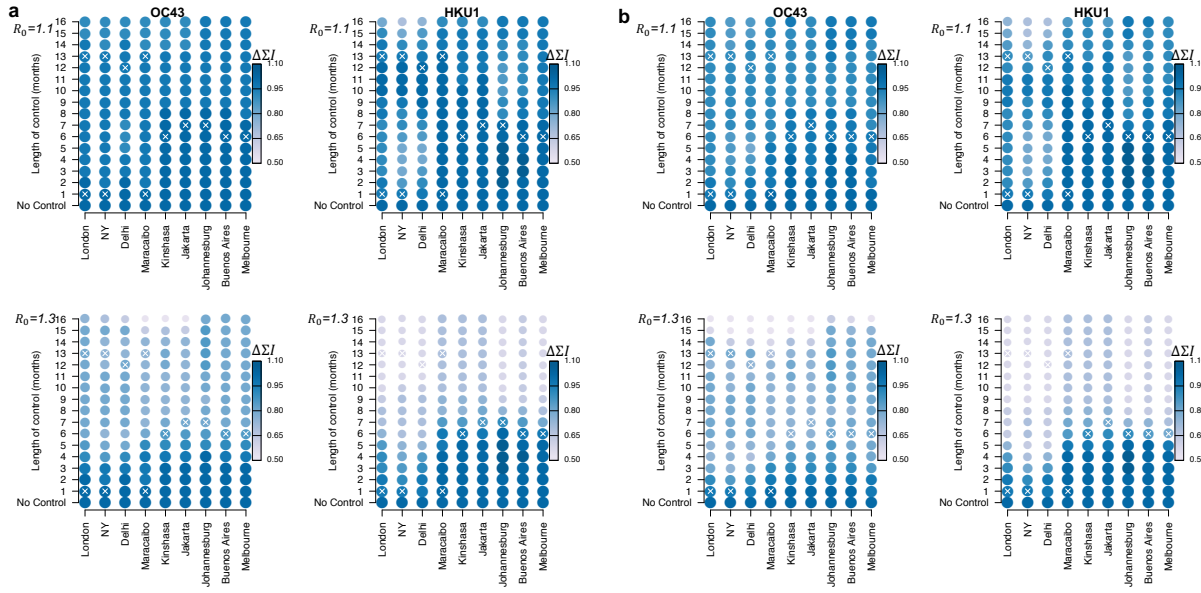


Figure S5: Impact of control on total infected. The relative (to the no-control scenario) effect of control measures on cumulative total infections by location where control measures begin at a) one month after the first infection or b) six weeks after the first infection.

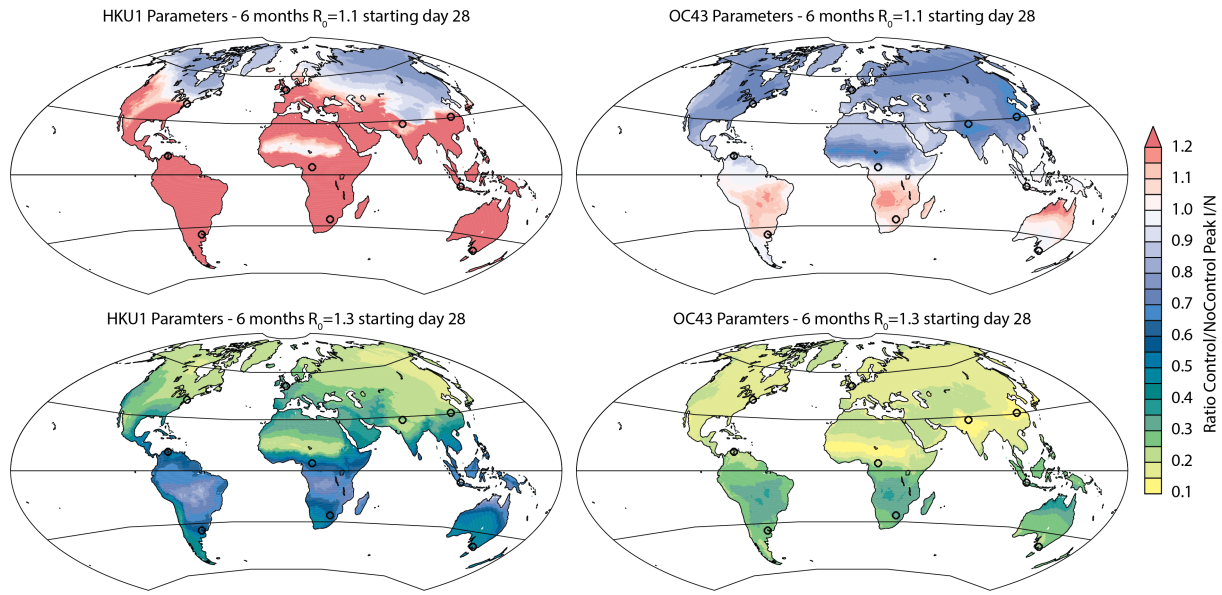


Figure S6: Map of relative I/N with control efforts at six months.) Map of relative change in peak incidence after six-months of controls using both the HKU1 and OC43 scenarios when $R_0 = 1.1$ and $R_0 = 1.3$.

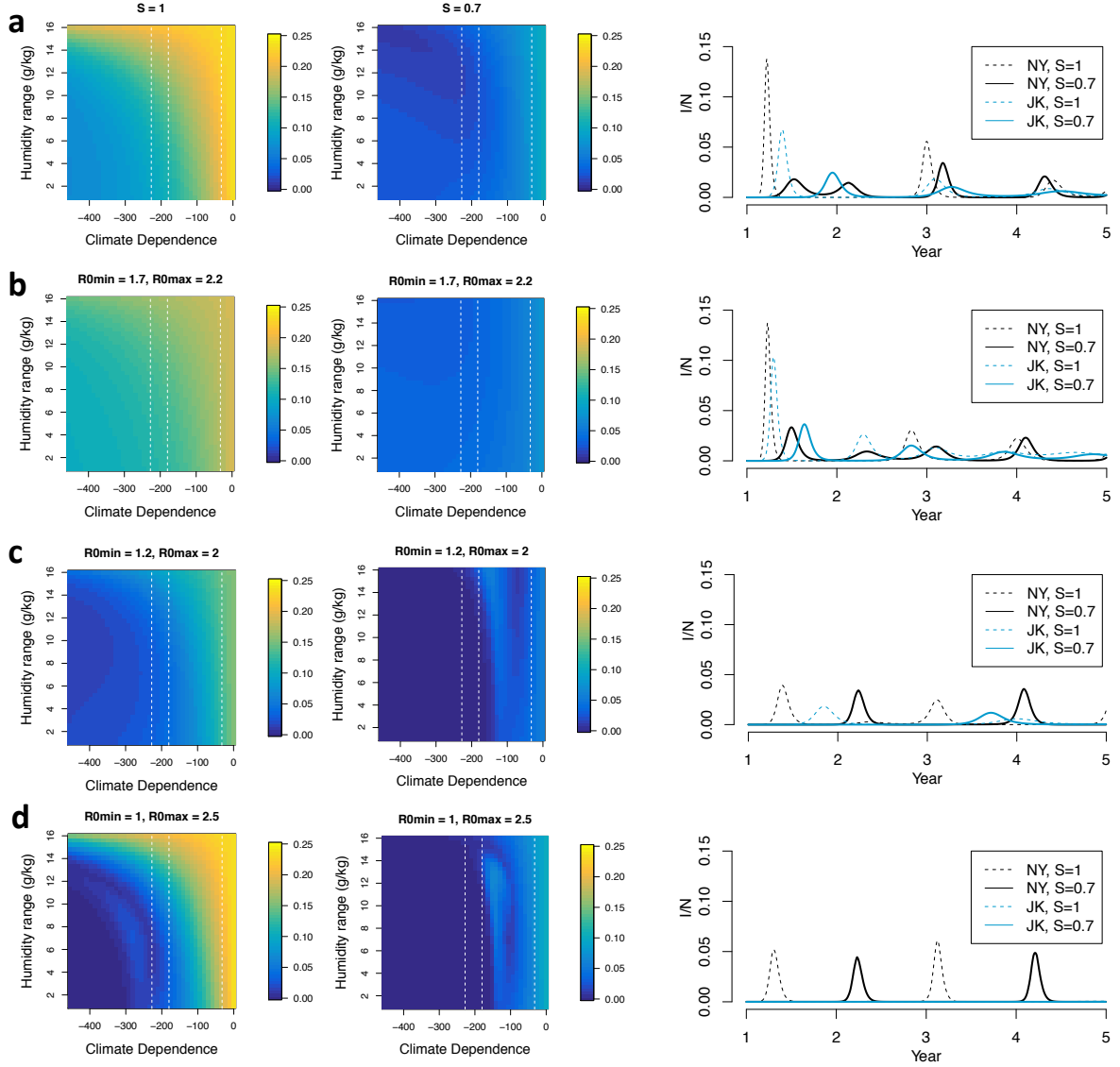


Figure S7: Sensitivity analysis. Image plots show peak I/N (within the six months) for different levels of climate dependence and humidity range with the proportion susceptible at the start of the simulation set to 1 (first column) or 0.7 (second column). The climate dependencies used in the scenarios in the main paper are shown with dashed lines. Values of $R_{0\min}$ and $R_{0\max}$ are allowed to vary across rows using a) $R_{0\min} = 1.5, R_{0\max} = 2.5$ i.e. our main model b) $R_{0\min} = 1.7, R_{0\max} = 2.2$ c) $R_{0\min} = 1.2, R_{0\max} = 2$ d) $R_{0\min} = 1, R_{0\max} = 2.5$. Simulated time series for New York (black) and Jakarta (blue) when $S = 1$ (dashed) and $S = 0.7$ (solid) and climate dependence/immunity is the same as HKU1 are shown in the right column.

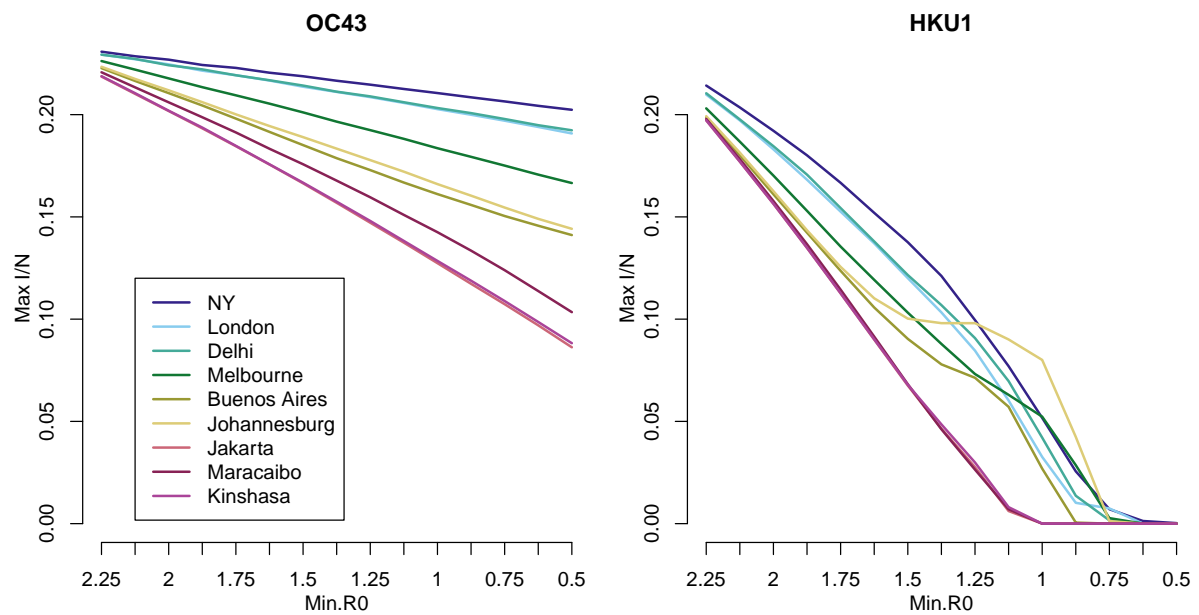


Figure S8: Sensitivity analysis. The effect of varying $R_{0\min}$ on peak I/N in the first year for different locations using OC43 and HKU1 climate dependence. $R_{0\max}$ is fixed at 2.5 and $R_{0\min}$ is varied.

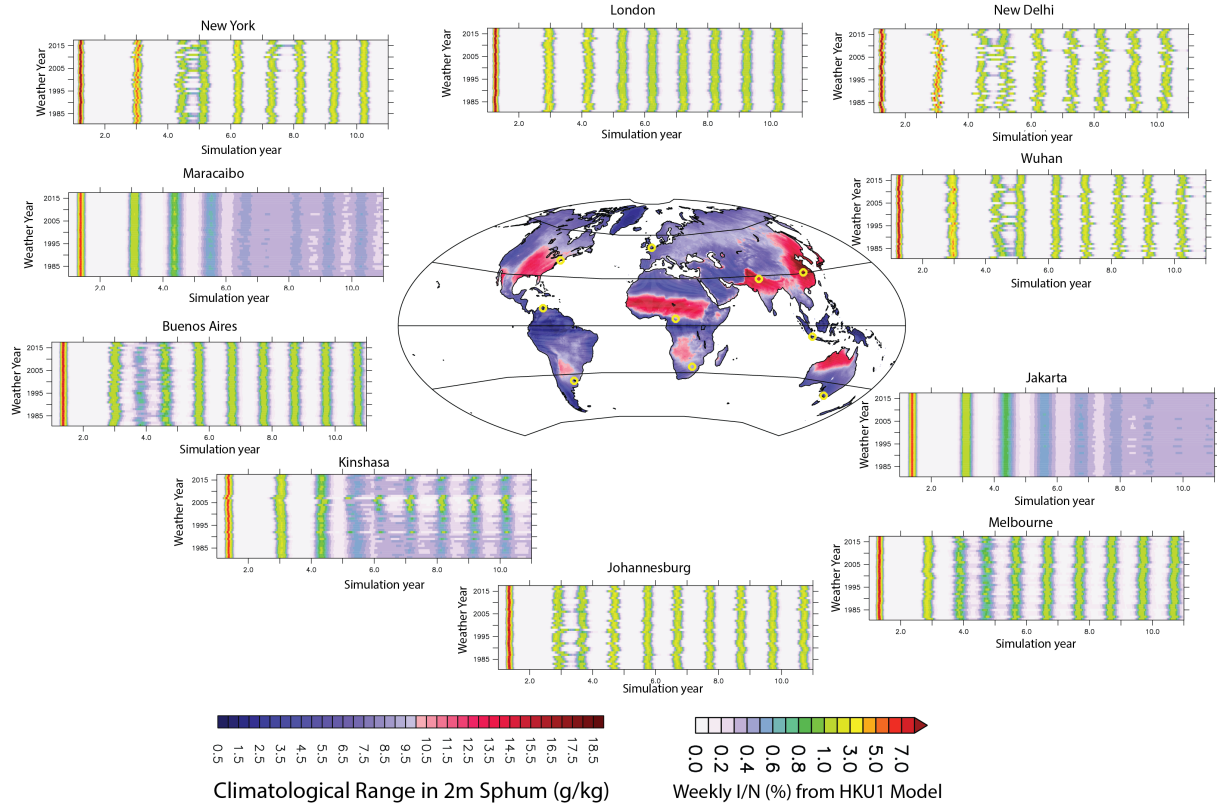


Figure S9: Sensitivity analysis. The effect of weather variability on pandemic peak size and endemic cycles, using HKU1 climate dependence.

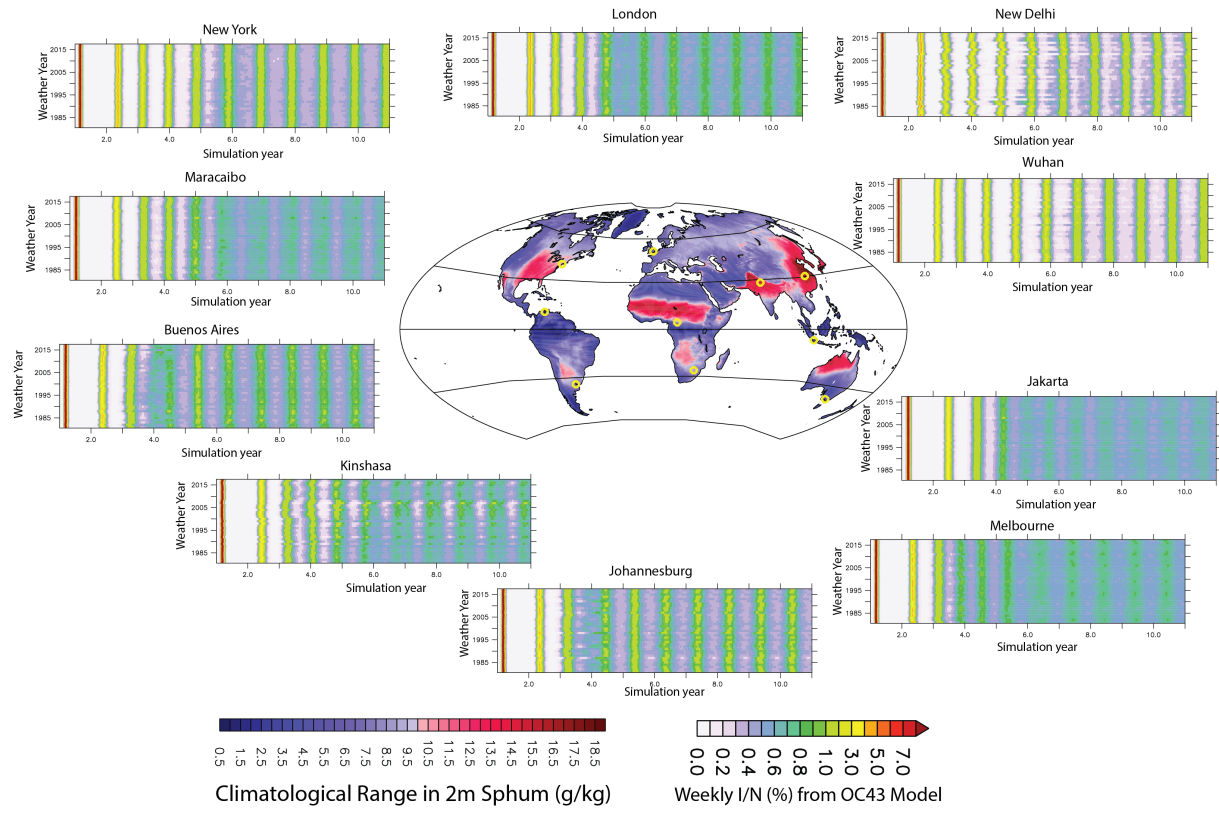


Figure S10: Sensitivity analysis. The effect of weather variability on pandemic peak size and endemic cycles, using OC43 climate dependence.

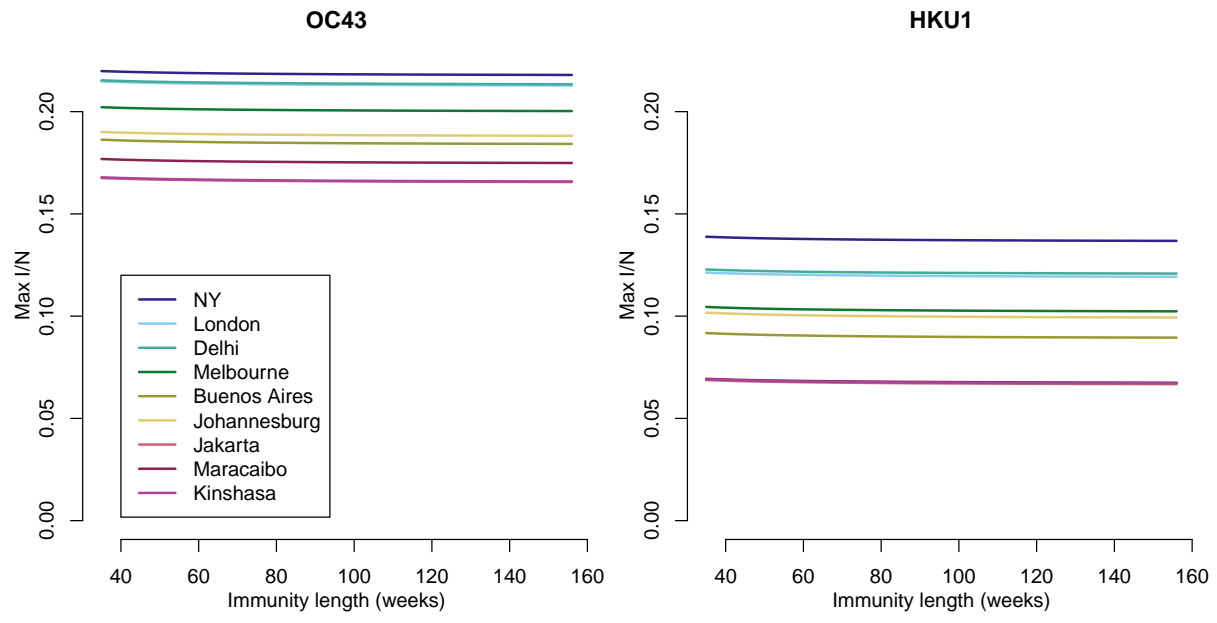


Figure S11: Sensitivity analysis. The effect of varying immunity length on peak I/N in the first year for different locations using OC43 and HKU1 climate dependence.

References and Notes

1. R. Verity, L. C. Okell, I. Dorigatti, P. Winskill, C. Whittaker, N. Imai, G. Cuomo-Dannenburg, H. Thompson, P. Walker, H. Fu, A. Dighe, J. Griffin, A. Cori, M. Baguelin, S. Bhatia, A. Boonyasiri, Z. M. Cucunuba, R. Fitzjohn, K. A. M. Gaythorpe, W. Green, A. Hamlet, W. Hinsley, D. Laydon, G. Nedjati-Gilani, S. Riley, S. van-Elsand, E. Volz, H. Wang, Y. Wang, X. Xi, C. Donnelly, A. Ghani, N. Ferguson, Estimates of the severity of COVID-19 disease. medRxiv 2020.03.09.20033357 [Preprint]. 13 March 2020; <https://doi.org/10.1101/2020.03.09.20033357>.
2. R. Li, C. Rivers, Q. Tan, M. B. Murray, E. Toner, M. Lipsitch, The demand for inpatient and ICU beds for COVID-19 in the US: lessons from Chinese cities. medRxiv 2020.03.09.20033241 [Preprint]. 16 March 2020; <https://doi.org/10.1101/2020.03.09.20033241>.
3. Q. Bukhari, Y. Jameel, Will coronavirus pandemic diminish by summer? SSRN 3556998 [Preprint]. 17 March 2020; <https://dx.doi.org/10.2139/ssrn.3556998>.
4. J. Wang, K. Tang, K. Feng, W. Lv, High temperature and high humidity reduce the transmission of COVID-19. SSRN 3551767 [Preprint]. 9 March 2020; <https://dx.doi.org/10.2139/ssrn.3551767>.
5. M. M. Sajadi, P. Habibzadeh, A. Vintzileos, S. Shokouhi, F. Miralles-Wilhelm, A. Amoroso, Temperature, humidity and latitude analysis to predict potential spread and seasonality for COVID-19. SSRN 3550308 [Preprint]. 5 March 2020; <https://dx.doi.org/10.2139/ssrn.3550308>.
6. W. Luo, M. S. Majumder, D. Liu, C. Poirier, K. D. Mandl, M. Lipsitch, M. Santillana, The role of absolute humidity on transmission rates of the COVID-19 outbreak. medRxiv 2020.02.12.20022467 [Preprint]. 17 February 2020; <https://doi.org/10.1101/2020.02.12.20022467>.
7. Y. Ma, Y. Zhao, J. Liu, X. He, B. Wang, S. Fu, J. Yan, J. Niu, B. Luo, Effects of temperature variation and humidity on the mortality of COVID-19 in Wuhan. medRxiv 2020.03.15.20036426 [Preprint]. 18 March 2020; <https://doi.org/10.1101/2020.03.15.20036426>.
8. R. E. Baker, A. S. Mahmud, C. J. E. Metcalf, Dynamic response of airborne infections to climate change: Predictions for varicella. *Clim. Change* **148**, 547–560 (2018). [doi:10.1007/s10584-018-2204-4](https://doi.org/10.1007/s10584-018-2204-4)
9. J. Shaman, M. Kohn, Absolute humidity modulates influenza survival, transmission, and seasonality. *Proc. Natl. Acad. Sci. U.S.A.* **106**, 3243–3248 (2009). [doi:10.1073/pnas.0806852106](https://doi.org/10.1073/pnas.0806852106) [Medline](#)
10. A. C. Lowen, J. Steel, Roles of humidity and temperature in shaping influenza seasonality. *J. Virol.* **88**, 7692–7695 (2014). [doi:10.1128/JVI.03544-13](https://doi.org/10.1128/JVI.03544-13) [Medline](#)
11. A. C. Lowen, S. Mubareka, J. Steel, P. Palese, Influenza virus transmission is dependent on relative humidity and temperature. *PLOS Pathog.* **3**, 1470–1476 (2007). [doi:10.1371/journal.ppat.0030151](https://doi.org/10.1371/journal.ppat.0030151) [Medline](#)

12. J. Shaman, V. E. Pitzer, C. Viboud, B. T. Grenfell, M. Lipsitch, Absolute humidity and the seasonal onset of influenza in the continental United States. *PLOS Biol.* **8**, e1000316 (2010). [doi:10.1371/journal.pbio.1000316](https://doi.org/10.1371/journal.pbio.1000316) Medline
13. R. E. Baker, A. S. Mahmud, C. E. Wagner, W. Yang, V. E. Pitzer, C. Viboud, G. A. Vecchi, C. J. E. Metcalf, B. T. Grenfell, Epidemic dynamics of respiratory syncytial virus in current and future climates. *Nat. Commun.* **10**, 5512 (2019). [doi:10.1038/s41467-019-13562-y](https://doi.org/10.1038/s41467-019-13562-y) Medline
14. V. E. Pitzer, C. Viboud, W. J. Alonso, T. Wilcox, C. J. Metcalf, C. A. Steiner, A. K. Haynes, B. T. Grenfell, Environmental drivers of the spatiotemporal dynamics of respiratory syncytial virus in the United States. *PLOS Pathog.* **11**, e1004591 (2015). [doi:10.1371/journal.ppat.1004591](https://doi.org/10.1371/journal.ppat.1004591) Medline
15. M. E. Martinez, The calendar of epidemics: Seasonal cycles of infectious diseases. *PLOS Pathog.* **14**, e1007327 (2018). [doi:10.1371/journal.ppat.1007327](https://doi.org/10.1371/journal.ppat.1007327) Medline
16. S. Takahashi, Q. Liao, T. P. Van Boeckel, W. Xing, J. Sun, V. Y. Hsiao, C. J. E. Metcalf, Z. Chang, F. Liu, J. Zhang, J. T. Wu, B. J. Cowling, G. M. Leung, J. J. Farrar, H. R. van Doorn, B. T. Grenfell, Hand, foot, and mouth disease in China: Modeling epidemic dynamics of enterovirus serotypes and implications for vaccination. *PLOS Med.* **13**, e1001958 (2016). [doi:10.1371/journal.pmed.1001958](https://doi.org/10.1371/journal.pmed.1001958) Medline
17. J. R. Gog, S. Ballesteros, C. Viboud, L. Simonsen, O. N. Bjornstad, J. Shaman, D. L. Chao, F. Khan, B. T. Grenfell, Spatial transmission of 2009 pandemic influenza in the US. *PLOS Comput. Biol.* **10**, e1003635 (2014). [doi:10.1371/journal.pcbi.1003635](https://doi.org/10.1371/journal.pcbi.1003635) Medline
18. S. M. Kissler, C. Tedijanto, E. Goldstein, Y. H. Grad, M. Lipsitch, Projecting the transmission dynamics of SARS-CoV-2 through the postpandemic period. *Science* eabb5793 (2020). [doi:10.1126/science.abb5793](https://doi.org/10.1126/science.abb5793) Medline
19. Centers for Disease Control and Prevention, Surveillance for common human coronaviruses (2020); www.cdc.gov/surveillance/nrevss/coronavirus/index.html.
20. L. Hoffmann, G. Günther, D. Li, O. Stein, X. Wu, S. Griessbach, Y. Heng, P. Konopka, R. Müller, B. Vogel, J. S. Wright, From ERA-Interim to ERA5: The considerable impact of ECMWF's next-generation reanalysis on Lagrangian transport simulations. *Atmos. Chem. Phys.* **19**, 3097–3124 (2019). [doi:10.5194/acp-19-3097-2019](https://doi.org/10.5194/acp-19-3097-2019)
21. NASA Socioeconomic Data and Applications Center (SEDAC), Gridded Population of the World, Version 4 (GPWv4): Population Density, Revision 11. Palisades, NY; <https://sedac.ciesin.columbia.edu/data/set/gpw-v4-population-density-rev11> [accessed March 2020].
22. S. W. Park, B. M. Bolker, D. Champredon, D. J. D. Earn, M. Li, J. S. Weitz, B. T. Grenfell, J. Dushoff, Reconciling early-outbreak estimates of the basic reproductive number and its uncertainty: framework and applications to the novel coronavirus (SARS-CoV-2) outbreak. medRxiv 2020.01.30.20019877 [Preprint]. 28 February 2020; <https://doi.org/10.1101/2020.01.30.20019877>.
23. M. Kamo, A. Sasaki, The effect of cross-immunity and seasonal forcing in a multi-strain epidemic model. *Physica D* **165**, 228–241 (2002). [doi:10.1016/S0167-2789\(02\)00389-5](https://doi.org/10.1016/S0167-2789(02)00389-5)

24. J. D. Tamerius, J. Shaman, W. J. Alonso, K. Bloom-Feshbach, C. K. Uejio, A. Comrie, C. Viboud, Environmental predictors of seasonal influenza epidemics across temperate and tropical climates. *PLOS Pathog.* **9**, e1003194 (2013). [doi:10.1371/journal.ppat.1003194](https://doi.org/10.1371/journal.ppat.1003194) [Medline](#)
25. R. E. Baker, rebaker64/climate-cov: R1. Zenodo (2020); [doi:10.5281/zenodo.3787766](https://doi.org/10.5281/zenodo.3787766).
26. M. E. Killerby, H. M. Biggs, A. Haynes, R. M. Dahl, D. Mustaquim, S. I. Gerber, J. T. Watson, Human coronavirus circulation in the United States 2014–2017. *J. Clin. Virol.* **101**, 52–56 (2018). [doi:10.1016/j.jcv.2018.01.019](https://doi.org/10.1016/j.jcv.2018.01.019) [Medline](#)
27. R. Gelaro, W. McCarty, M. J. Suárez, R. Todling, A. Molod, L. Takacs, C. Randles, A. Darmenov, M. G. Bosilovich, R. Reichle, K. Wargan, L. Coy, R. Cullather, C. Draper, S. Akella, V. Buchard, A. Conaty, A. da Silva, W. Gu, G.-K. Kim, R. Koster, R. Lucchesi, D. Merkova, J. E. Nielsen, G. Partyka, S. Pawson, W. Putman, M. Rienerer, S. D. Schubert, M. Sienkiewicz, B. Zhao, The Modern-Era Retrospective Analysis for Research and Applications, Version 2 (MERRA-2). *J. Clim.* **30**, 5419–5454 (2017). [doi:10.1175/JCLI-D-16-0758.1](https://doi.org/10.1175/JCLI-D-16-0758.1) [Medline](#)
28. L. Bao, W. Deng, H. Gao, C. Xiao, J. Liu, J. Xue, Lv. Qi, J. Liu, P. Yu, Y. Xu, F. Qi, Y. Qu, F. Li, Z. Xiang, H. Yu, S. Gong, M. Liu, G. Wang, S. Wang, Z. Song, Y. Liu, W. Zhao, Y. Han, L. Zhao, X. Liu, Q. Wei, C. Qin, Lack of reinfection in rhesus macaques infected with SARS-CoV-2. bioRxiv 2020.03.13.990226 [Preprint]. 1 May 2020; <https://doi.org/10.1101/2020.03.13.990226>.
29. K. A. Callow, H. F. Parry, M. Sergeant, D. A. Tyrrell, The time course of the immune response to experimental coronavirus infection of man. *Epidemiol. Infect.* **105**, 435–446 (1990). [doi:10.1017/S0950268800048019](https://doi.org/10.1017/S0950268800048019) [Medline](#)